ELSEVIER

Journal of Power Sources 76 (1998) 19–29

JOURNAL OF POWER SOURCES

In situ Scanning Electron Microscopy (SEM) observation of interfaces within plastic lithium batteries

F. Orsini [a], A. Du Pasquier [a], B. Beaudoin [a], J.M. Tarascon [a,*], M. Trentin [b], N. Langenhuizen [c], E. De Beer [c], P. Notten [c]

[a] *Laboratoire de Réactivité et de Chimie des Solides, UPRES-A 6007, Université de Picardie Jules Verne, 33 rue Saint-Leu, F-80039 Amiens Cédex, France*

[b] *Philips Electronique Industrielle S.A.S., 22 avenue Descartes, 94454 Limeil-Brévannes Cédex, France*

[c] *Philips Research Laboratories, Prof. Hostlaan 4, 5656 AA Eindhoven, Netherlands*

Received 15 May 1998; accepted 22 June 1998

Abstract

Cross-sections of plastic rechargeable Li-cells were observed in a quasi in situ mode by means of a scanning electron microscope. All cells were composed of a composite cathode, containing $LiMn_2O_4$ as active material, and of a hybrid polymer electrolyte consisting of a polymer matrix embedded with a solution of lithium salt. At the negative side, three kinds of anodes (Li, Cu and graphite) were successively used. The influence of the current density on the morphology of the lithium deposit was studied from these three different configurations. Scanning Electron Microscopy (SEM) evidences for (1) the accumulation of mossy lithium, and (2) the Li-dendrites growth at the interface between Li and electrolyte are given, and correlated to the poor cell cyclability. This deterioration of the interface was confirmed by AC-impedance measurements.

Keywords: Secondary lithium battery; Lithium electrode; Morphology; Dendrite

1. Introduction

The development of the portable electronics market requires high energy density batteries. While being theoretically the most promising, rechargeable batteries based on Li as the negative electrode encounter difficulties to reach the market place, because of safety and cyclability issues. These problems are associated to the reactivity of Li and to the growth of dendrites at the Li^0-anode upon cycling [1]. Thus, solving the dendrite growth at the metallic lithium electrode remains a serious challenge.

A partial solution to this problem that consists of using a polymeric electrolyte rather than a liquid electrolyte was proposed two decades ago [2]. However, the application of these batteries will be limited to high temperatures ($> 80°C$) because of the limited ionic conductivity of the polymer electrolyte at room temperature. Thus, while already intensely studied, we decided to further address the non-uniform Li-plating issue, by means of advanced techniques such as electron microscopy, X-ray microanalysis, and impedance spectroscopy. More precisely, we studied the lithium deposition process on Li, Cu and graphite at different current densities to better understand the mechanism of the dendrite growth. Indeed, it has been shown that the morphology of the Li-deposit depends on both the current density [3] and the native state of the metallic surface [4]. More specifically, the reactivity of the lithium with the organic electrolytes leads to a passivating layer whose thickness and nature influence the further Li deposition [5–8]. Besides the correlations current densities/dendrites and passivating layer/dendrites, some authors tried to precisely explain the mechanism of the dendritic deposition [9]: the velocity of the anions, the gradient of salt concentration and the motion of the electrolyte were related to a theoretical model of the dendrite growth.

Studies of lithium surfaces by microscopy techniques such as Scanning Electron Microscopy (SEM) or Atomic

* Corresponding author. Tel.: +33-3-2282-7571; Fax: +33-3-2282-7590; E-mail: jean-marie.tarascon@sc.u-picardie.fr

0378-7753/98/$19.00
PII: S0378-7753(98)00128-1

Force Microscopy (AFM) have already been done [10,11]. However, most of these studies were carried out on lithiated surfaces that were shortly exposed to air during the transfer from the electrochemical cell to the microscope antechamber, therefore risks of surface contamination were always present. In this paper, we report high quality images obtained from a Field Emission Gun (FEG) microscope on pristine surfaces/interfaces. Air exposure was prevented with a special system designed by Philips, which allowed the transfer of the cell from a glove box into the SEM by means of a movable airlock. Moreover, the sample was cooled down ($\sim -20°C$) to prevent any damage or electrolyte evaporation due to the vacuum in the antechamber during the observation. Finally, this equipment allowed us to observe cell cross-sections without preparation, since the cooling system spared us any washing and drying, usually necessary to obtain a sufficient vacuum value in a reasonable time.

The battery samples used in the present study were made by the plastic laminate technology [12]. With such a configuration, the interfaces were observable just after a simple cut with a razor blade.

2. Experimental

All the cells were assembled according to Bellcore's plastic Li-ion technology, using as separator a copolymer matrix (Polyvinylidene fluoride(PVdF)–Hexafluoropropylene(HFP)) mixed with SiO_2 as filler, and dibutyl phtalate (DBP) as plasticizer. The 15×15 mm^2 plastic cathode laminates were prepared outside the glove box from a mixture of $LiMn_2O_4$ (homemade), PVDF–HFP copolymer, DBP, and carbon black. The cathode laminate together with an aluminium grid on one side, and the separator on the opposite side, were fed through a heated double-roll laminator to produce the cathode-separator laminate, common to all the cells investigated. This laminate was coupled with lithium, copper or graphite anode to produce what will be denoted in the following as *lithium batteries* (Fig. 1a), *copper cells* (Fig. 1b), and *lithium ion*

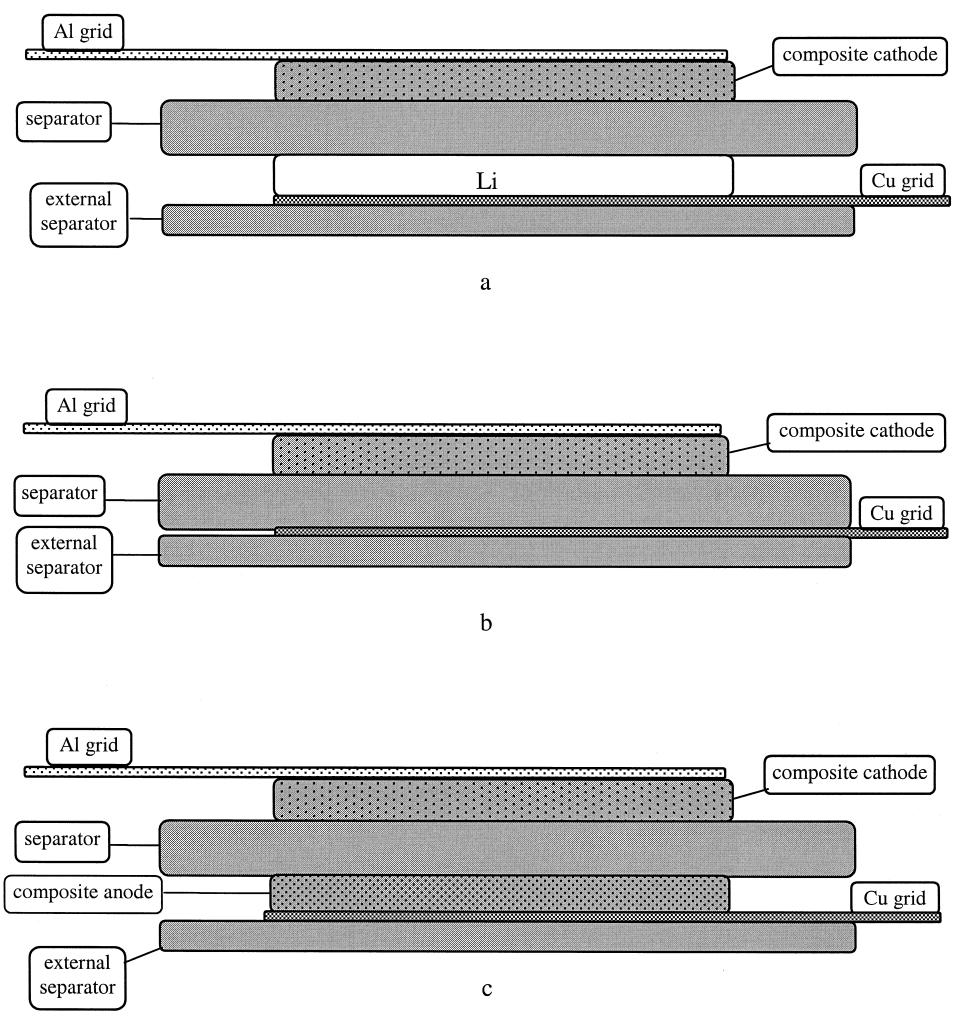

Fig. 1. Schematic cross-section of (a) lithium battery, (b) copper cell, (c) lithium ion battery.

batteries (Fig. 1c), respectively. After the DBP extraction by means of ether, the cells were swollen in an EC/DMC mixture (2/1 in weight ratio) containing a dissolved salt ($LiPF_6$ 1 M).

More specifically, the lithium batteries were assembled in an argon glove box as follows: the anode (15×15 mm^2 Li-foil) was first laminated at 150°C with its collector (a Cu grid). Then a few drops of NMP (1-methyl-2-pyrrolidinone) were deposited onto the lithium surface to enhance the further polymer adhesion onto metallic lithium. The cathode-separator laminate, previously DBP-extracted, was manually pressed onto the anode. The obtained cell was then impregnated with the liquid electrolyte. After 30 min, the electrolyte activation was completed and the battery was laminated at 130°C with an additional external polymer laminate on the Li side. This extra layer was used to obtain a better polymer/metal contact. Afterwards, the cell was sealed in a hermetic bag and taken out of the glove box to be cycled.

The copper cells were fully assembled outside the glove box by laminating a 15×15 mm^2 Cu-grid with the cathode part on the separator side. Note that the active area of the grid was 50% lower than 15×15 mm^2, calculated by considering the mesh size and the internal wall area. Once the DBP was extracted, the cell was placed into an argon dry-box for electrolyte activation, and then sealed in an air-tight plastic bag prior to testing.

For the lithium ion batteries, plastic anode laminates were made from carbon microbeads MCMB 2528 (Osaka Gas). In that case, a copper grid as current collector, the carbon-based negative electrode, and the cathode separator part were fed through a heated double-roll laminator to produce a single cell laminate that was extracted for its DBP content prior to be placed into the dry-box for activation, and sealing as detailed elsewhere [13].

The electrochemical cells were cycled by means of a Mac Pile system (Biologic, Claix, France) operating in a galvanostatic mode. Current densities were comprised between 0.22 ($C/10$) and 2.2 mA/cm^2 ($C/1$), while the voltage limits were fixed at 3.5 and 4.5 V (or 4.6 V). Electrochemical Impedance Spectroscopy (EIS) measurements were performed with a PGSTAT 20 Autolab instrument (Eco Chemie). The spectra were acquired at various stages of the cell charge or discharge in a frequency range of 50 mHz to 1 MHz, using a perturbation voltage amplitude of 5 mV.

The microscopy studies were performed by means of a Philips XL30 FEG–SEM coupled with an Oxford X-ray microanalyzer (Link Isis). The sample transfer attachment system was designed, built, and installed by Philips (Scheme 1). It is composed of two parts: a *fixed airlock* attached to the microscope, and a *removable airlock* that can be introduced into a glove box. The subsequent steps for a cell SEM investigation are listed below. The sealed

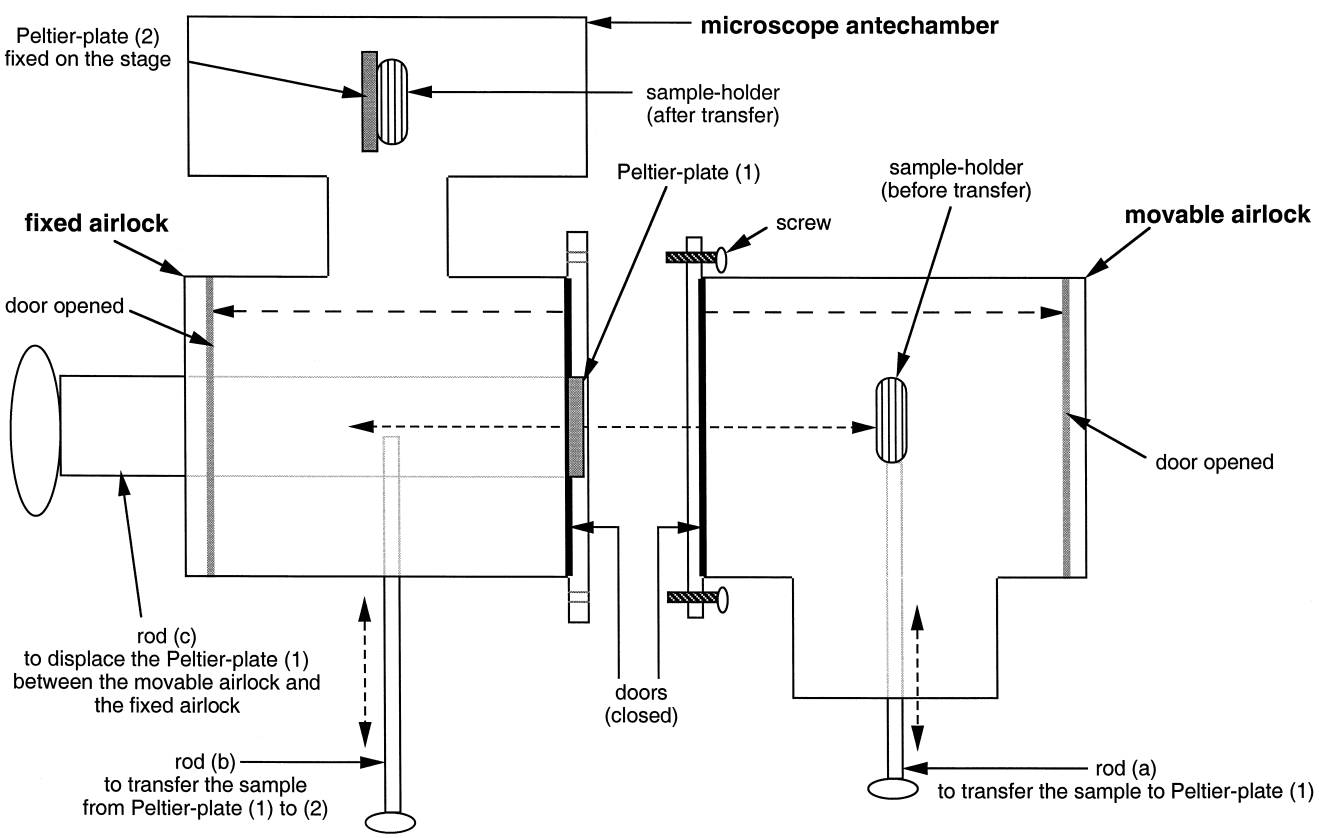

Scheme 1. Simplified representation of the transfer system (top view) (the dashed arrows indicate the motions of the different pieces).

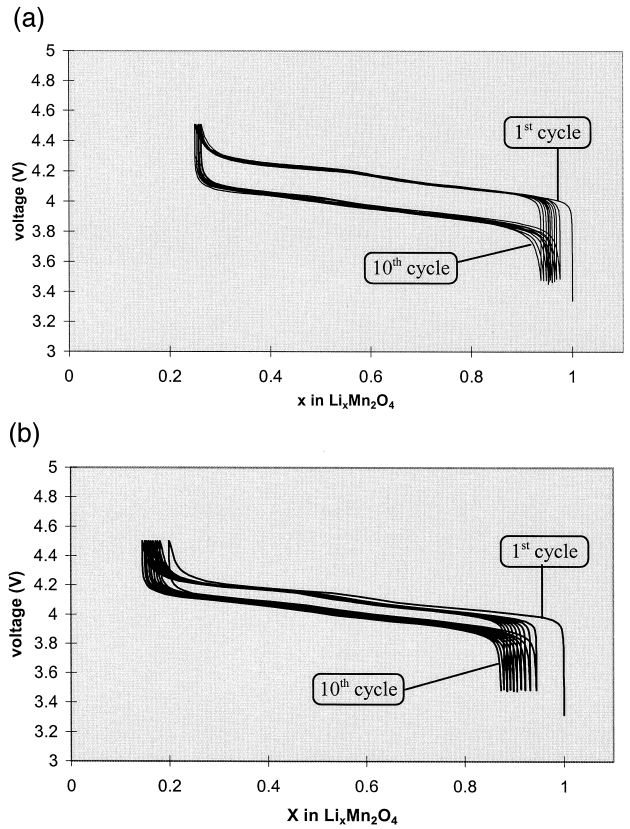

Fig. 2. (a)Galvanostatic cycling curves at $C/5$ (0.45 mA/cm^2) of a lithium battery. (b) Galvanostatic cycling curves at $C/10$ (0.22 mA/cm^2) of a lithium battery.

cell, which was cycled outside the glove box, was put into the argon atmosphere. Its hermetic bag was removed, and the battery was cut with a razor blade in order to reveal its internal section. Then it was fixed to the sample-holder which was screwed to the rod (a) of the movable airlock. Afterwards this airlock was closed, taken out of the glove box and screwed to the fixed airlock. Then the door of the fixed airlock was opened so that the small amount of air present between both doors was evacuated by means of the microscope's pumps. Then the fixed airlock was closed again, and the door of the movable airlock was completely opened. Afterwards the Peltier-plate (1) was put into the movable airlock by means of the rod (c), and the battery was transferred onto this Peltier-plate (1) by means of the rod (a). The sample was then cooled down in order to freeze the liquid part of the electrolyte (which will stay in the cell during the observation under vacuum). After 15 min, the door of the fixed airlock was opened to evacuate the movable airlock by means of the microscope pumping system, and the Peltier-plate (1) (holding the sample) was moved into the fixed airlock in front of the rod (b). The final step was the transfer of the sample from the Peltier-plate (1) to the Peltier-plate (2) of the microscope antechamber by means of the rod (b). When the vacuum was low enough, the high voltage of the SEM was switched on (typically 2 kV).

3. Results

3.1. Lithium batteries

The laminated cells were cycled at different current densities. Fig. 2 shows voltage curves for several cycles at $C/5$ and $C/10$. A hysteresis between the charging and

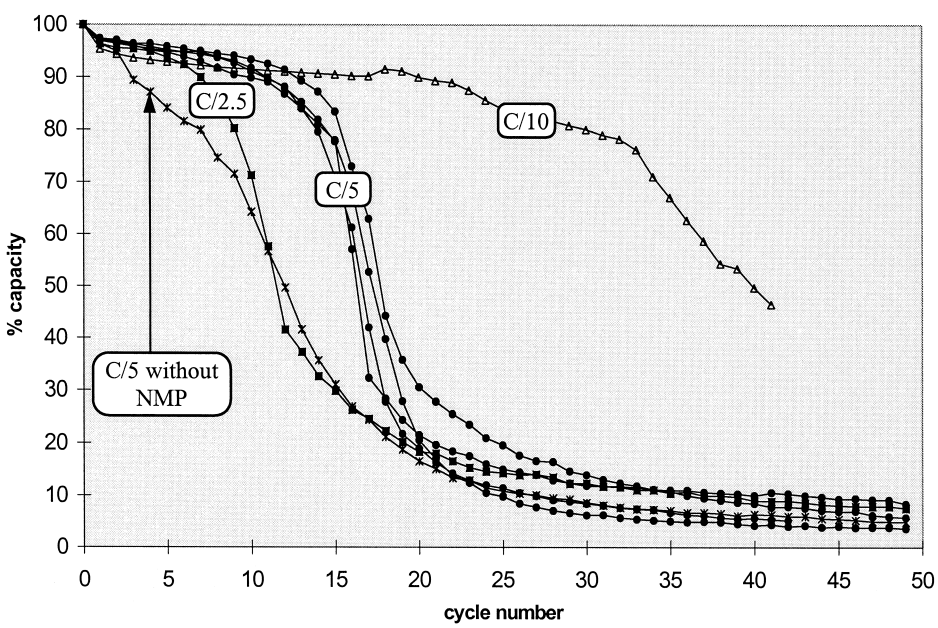

Fig. 3. Capacity vs. cycle number for lithium batteries at different cycling rates.

discharging curves was always observed. As expected, the polarization decreases with decreasing cycling rate. The influence of the current densities on the capacity during cycling is shown Fig. 3. Note that lower the current density, smaller the capacity loss. For instance, within the present cell configuration, by changing the current rate from $C/2.5$ to $C/10$, 35 instead of 10 cycles could be achieved. Regarding the $C/5$ cycling rate, a drastic capacity loss appeared after 15 cycles, suggesting dramatic interfacial reactions within the cell. It was then of great importance to study such cells which present moreover a good reproducibility of the cycling performances, as shown by the four $C/5$ batteries tested. Finally Fig. 3 also shows the beneficial effect of the NMP by comparing the 'cell without NMP' with the other batteries cycled at the same rate of $C/5$.

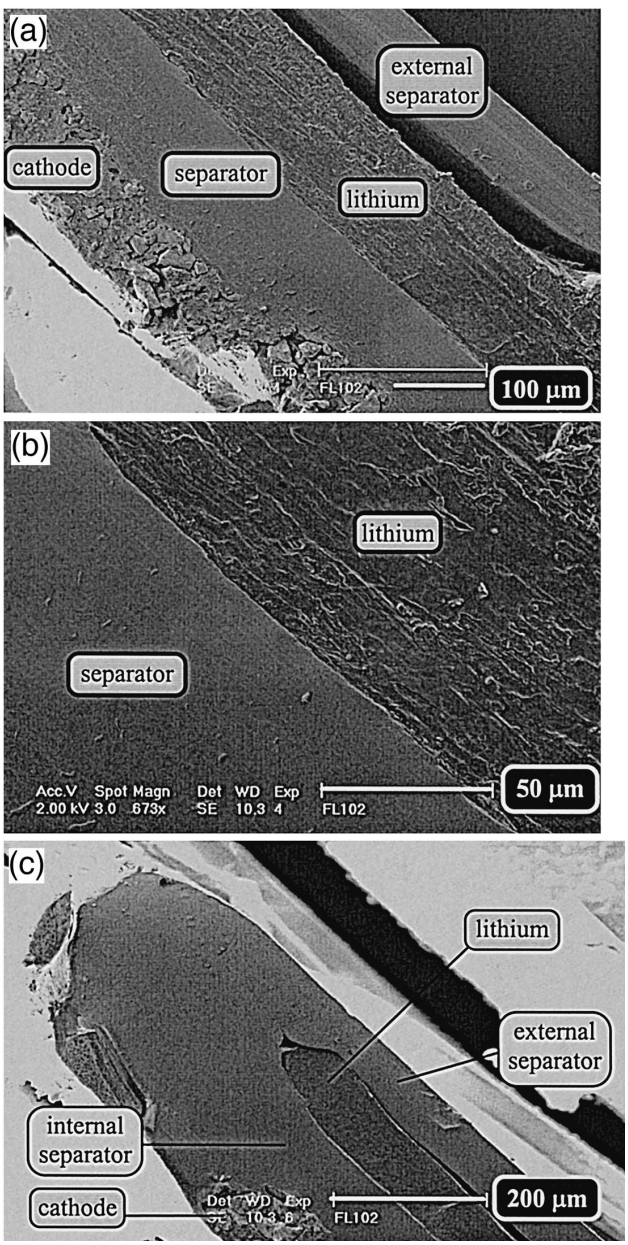

Fig. 4. (a) Cross-section of a non-cycled lithium battery. (b) Li/polymer electrolyte interface of a non-cycled lithium battery. (c) Section tip of a non-cycled lithium battery.

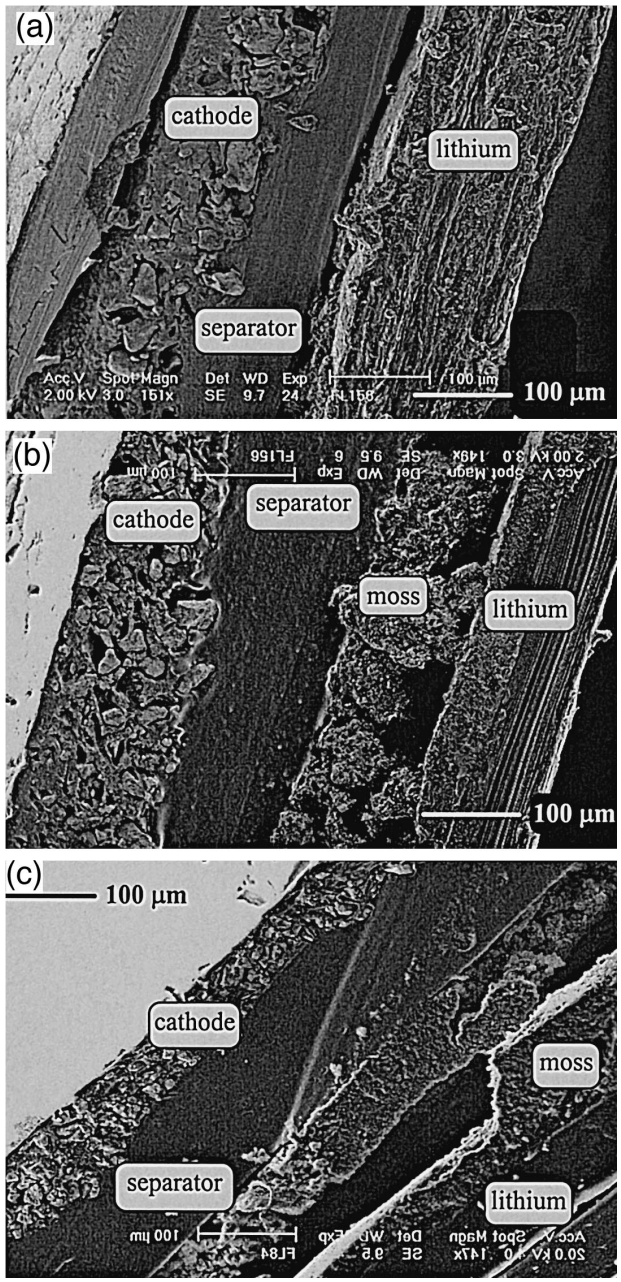

Fig. 5. (a) Lithium battery section after the 1st charge ($C/5$, 0.45 mA/cm^2). (b) Lithium battery section after the 14th charge ($C/5$, 0.45 mA/cm^2). (c) Lithium battery section after the 50th charge ($C/5$, 0.45 mA/cm^2).

Fig. 4 shows cross-section micrographs of a non-cycled battery. The different parts of the cell, directly noted in the figure, were identified by means of X-ray microanalysis. The $LiMn_2O_4$ particles embedded in the composite cathode are well visible in Fig. 4a, while the separator presents a smoother cross-section. One can also note the difference

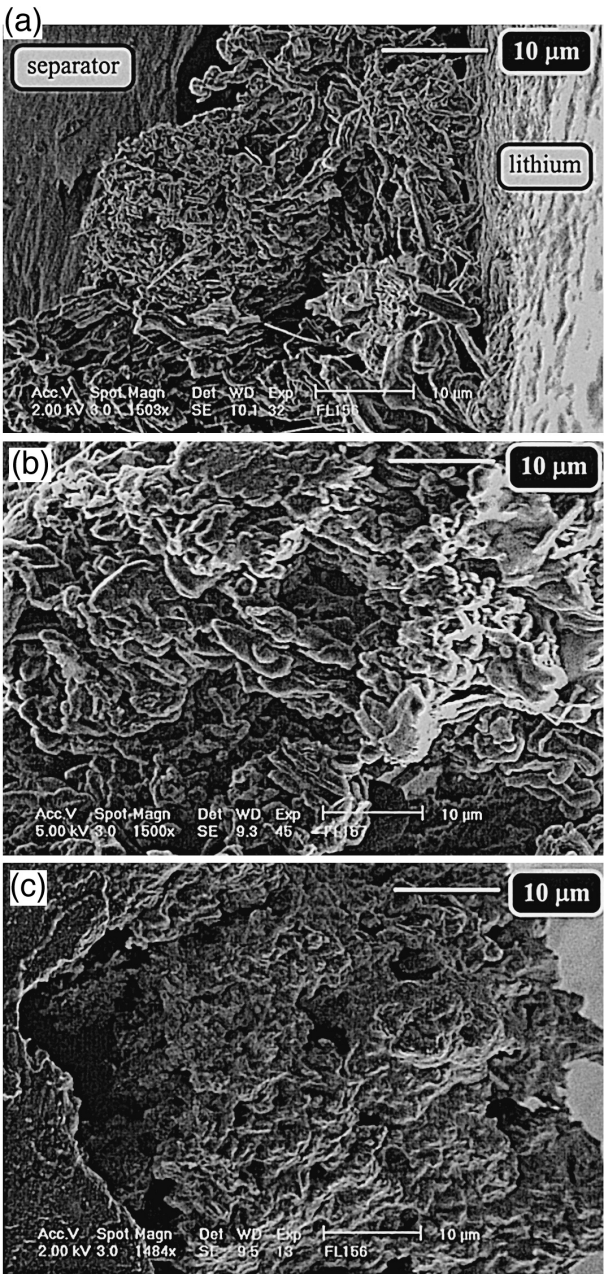

Fig. 6. Moss formed at the Li/separator interface of lithium batteries ($C/5$, 0.45 mA/cm^2) (a) 1st charge, (b) 14th charge, (c) 50th charge.

between the Li/separator and the Li/(external separator) interface: the external separator becomes separated from the lithium that was not NMP treated on that side. The Li/separator boundary very distinctly appears in the zoomed picture (Fig. 4b). The efficiency of the last lamination step consisting in melting external and internal separators can be visualized on Fig. 4c that displays the tip of a laminated battery.

An investigation of identical cells cycled at $C/5$ (0.45 mA/cm^2) was carried out. Fig. 5 shows cross-sections of lithium batteries stopped after the first, the 14th and the 50th charges. The images revealed that the Li/separator interface more and more deteriorated. However, other parts of the cells remained unaffected by the cycling. SEM pictures also indicated that a moss has formed at the

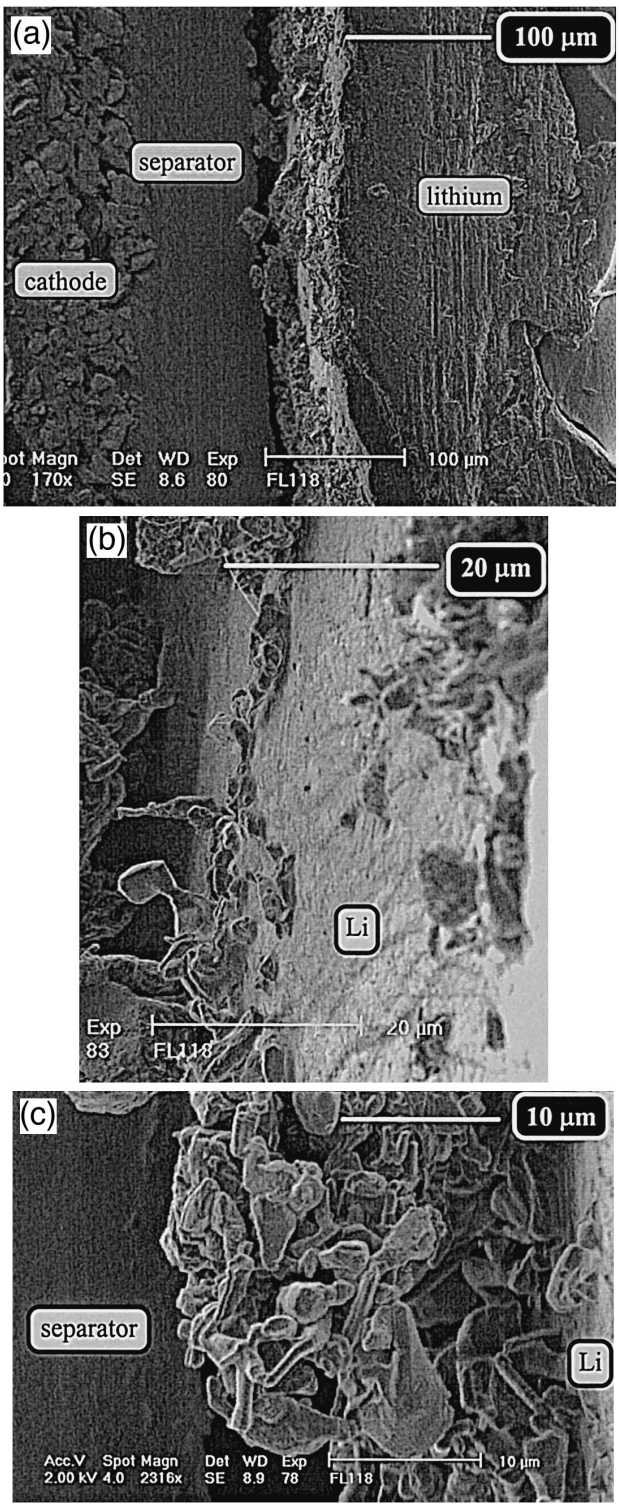

Fig. 7. (a) Section of a lithium battery after one charge at C (2.2 mA/cm^2). (b) Surface of the Li-anode of a lithium battery after one charge at C (2.2 mA/cm^2). (c) Li-deposit on the lithium surface after one charge at C (2.2 mA/cm^2).

Li/separator interface. Thus, the moss caused the separator disconnection from the lithium which became isolated from the polymer electrolyte. This drastic deterioration of the interface seemed to be the reason for the rapid capacity decrease observed for that cell. This effect was strongly enhanced with increasing the cycle number so that after 50 cycles (Fig. 5c) a very thick mossy layer has formed. In this extreme case, one should be aware that the cutting and the cooling of the battery could accentuate the poor appearance of the interface, and could explain the large empty space between the lithium and the separator. The morphology of the mossy layers, which were mainly the Li-deposits during the charge(s), is shown in Fig. 6. After one charge the moss appeared porous and probably crystallized, while it was more and more compact for the further charges. The effect of the cycling is then the formation of a more and more important amount of moss, whose morphology slowly changed to a more dense texture.

To observe the growth of true dendrites, similar experiments were carried out on lithium batteries cycled at higher current rates. The polarization was larger, and the capacity decrease faster than for a $C/5$ cycling rate. After one charge to 4.5 V corresponding to the extraction of 0.65 Li from the Mn-spinel, the cell was cut, transferred, and observed within the SEM. Fig. 7a shows a general view of the cell section, which presents an inhomogeneous Li/separator interface. After only one charge (lithium deposition) the lithium surface was already pushed aside from the separator, due to the growth of the lithium deposits at the lithium–polymer interface that are visible at a higher magnification in Fig. 7b and c. More precisely two kinds of lithium deposits can be distinguished on the Li-surface: aggregates (Fig. 7c) and tangled dendrites (Fig. 8). Note that the morphology of the aggregate looks like the moss deposited during a first charge at $C/5$ (Fig. 6a). According to the Li-surface state and to the separator/Li contact, the lithium plating led either to true dendrites or to aggregates. Nevertheless these aggregates seemed to be 'pressed dendrites' which could not grow freely. This assumption is uncertain because of the poor physical pressure applied by the separator against the lithium. Finally the shape of the deposits reported here is comparable with previous studies [9]. However, rarely has such a three-dimensional aspect of the dendrites in a complete battery been so clearly observed.

3.2. Copper cells

To determine the importance of the substrate, we decided to study the phenomena of Li-plating on copper instead of lithium. Copper cells were cycled at a low rate ($C/10$) to obtain a current density (0.45 mA/cm^2 of Cu) comparable to a lithium battery cycled at $C/5$. A typical galvanostatic cycling curve is shown in Fig. 9. Fresh and cycled cells were then observed by SEM to determine the morphology of the deposited lithium. For the non-cycled cell, the lithium-free Cu grid was embedded in the electrolyte polymer, which was completely fused with the cathode-separator part, and the copper/separator interface was well defined (Fig. 10). After one charge (Fig. 11) a moss appeared that tends to push the separator away, as in the case of the lithium batteries. The EDS spectra of this moss as well as its morphology were similar to those observed upon cycling for the lithium batteries. The influence of the lithium plating rate on its morphology was also

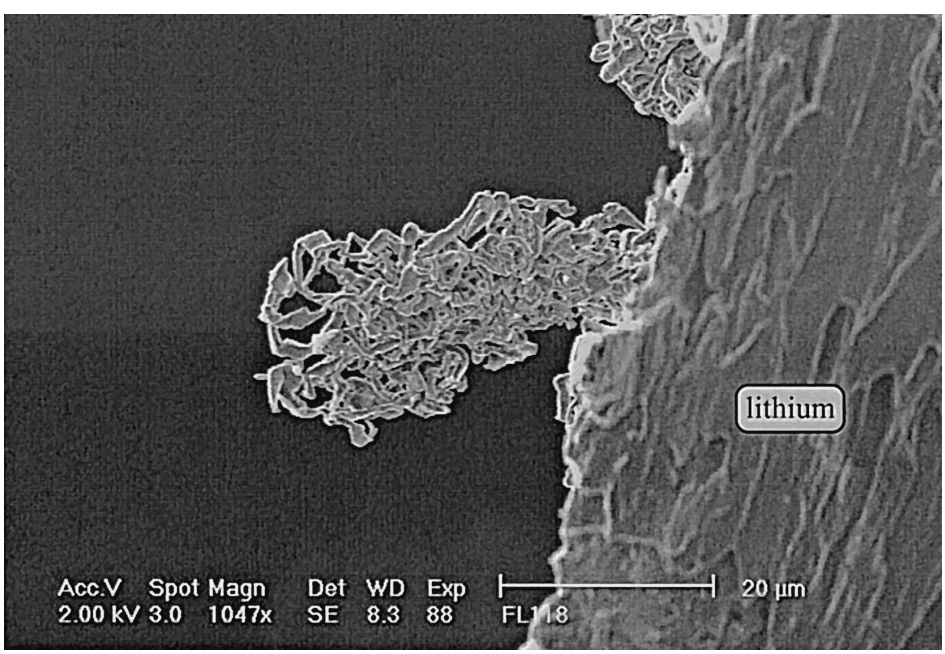

Fig. 8. Dendrite formed in a lithium battery after one charge at 2.2 mA/cm^2.

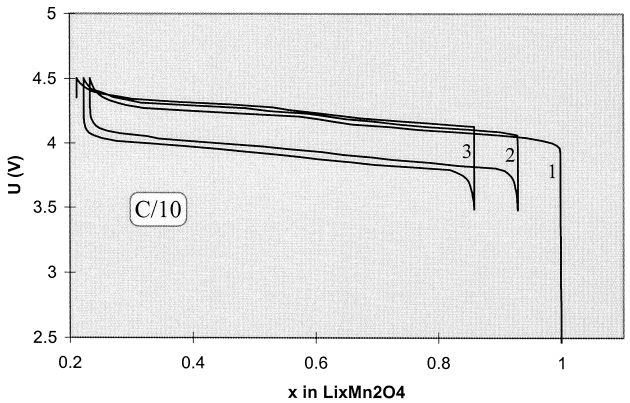

Fig. 9. Galvanostatic cycling curves at $C/10$ (0.45 mA/cm^2) of a copper cell.

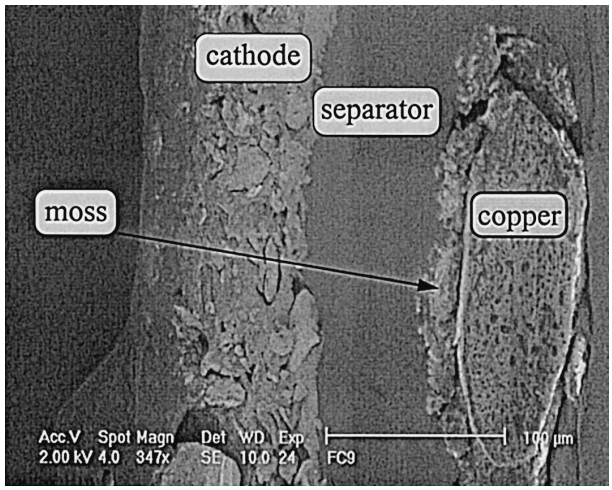

Fig. 11. Copper cell section after one charge at $C/10$ (0.45 mA/cm^2).

studied, and reported in Fig. 12 for a plating performed at a current density of 2.6 mA/cm^2, value also calculated by considering the active copper area. Note that the interface was more dendritic than a moss, and presented relative sharp bulges. However no true dendrites were observed. The current density being slightly higher than 2.2 mA/cm^2, value at which dendritic deposits were observed with the lithium batteries, it means that dendrites cannot as easily grow on Cu as on Li.

3.3. Lithium ion battery

A non-balanced lithium ion battery (e.g., carbon limited) was assembled in order to cause lithium plating on the graphite particles of the anode. The cells were cycled at a *C*-rate, value at which a dendritic deposition was observed within the lithium batteries (C, 2.2 mA/cm^2). However, in the case of the lithium ion battery, the actual current density reported for the anode, and calculated from the specific area of the graphite particles, was much ($200\times$) smaller than 2.2 mA/cm^2. After the first charge (i.e, the first Li plating was terminated), the procedure to observe the cell interfaces was carried out. The different components of the cell stacking can be clearly identified as indicated in Fig. 13a. A zoom of the graphite particles (Fig. 13b) indicates an apparent roughness that might be characteristic of the lithium plating, but no clear difference was observed in comparison with a non-cycled cell. Further experiments using larger current densities in order to observe dendritic growths on the graphite were unsuccessfully performed. However our cycling instruments can not deliver a sufficiently high absolute current to obtain current densities comparable to 2.2 mA/cm^2 (towards graphite particles).

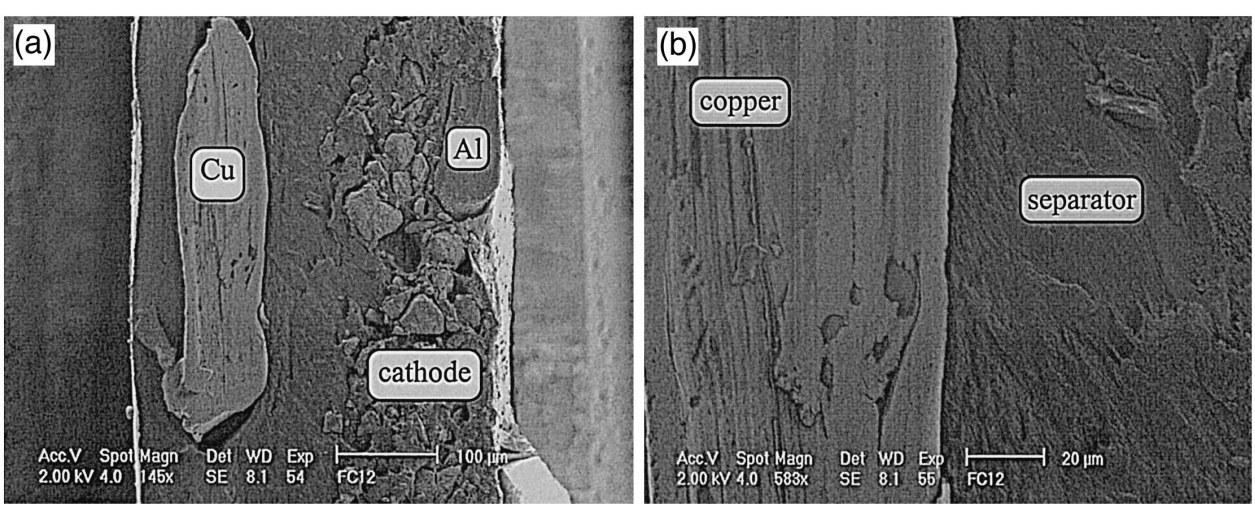

Fig. 10. Cross-section (a) and Cu/electrolyte interface (b) of a non-cycled copper cell.

4. Comparison of the three types of cells

Table 1 summarizes the different morphologies observed at the anodes for the three tested cells. For both the lithium batteries and the copper cells, a common result is that a low current density led to a mossy lithium deposition. At higher current densities, the deposit becomes more and more dendritic and true dendrites were observed at 2.2 mA/cm^2 in the case of the lithium batteries. Concerning the lithium ion battery, no specific morphology was observed at different cycling rates with a non-balanced (graphite-deficient) cell. This result is not surprising because the actual value of the current density vs. graphite was always very low, even if the cycling rate was large.

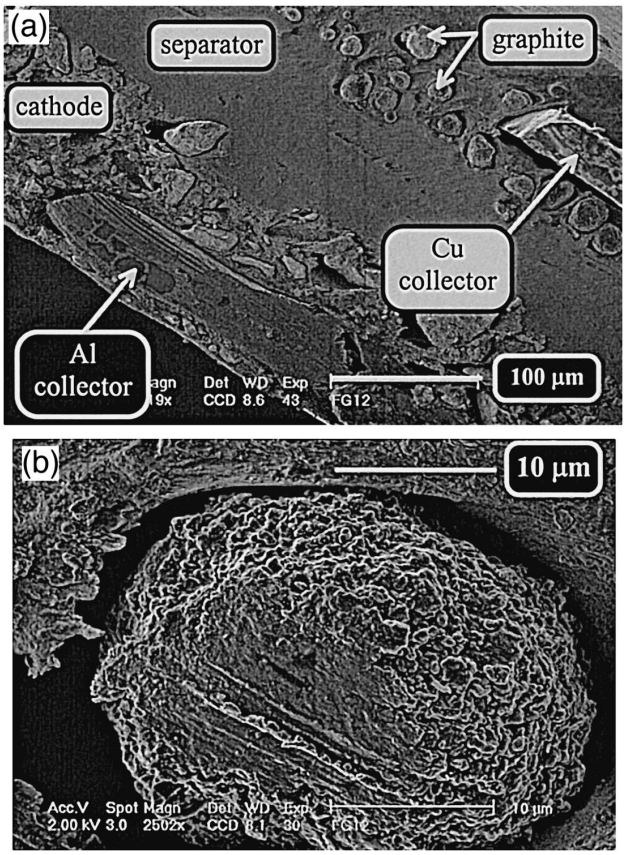

Fig. 13. (a) Cross section of a lithium ion battery. (b) Graphite particle of a lithium ion battery after one charge at *C*.

5. Discussion

We reported semi in situ SEM observations of lithium-cell cross-sections. A similar SEM transfer technique has been previously used by Aurbach et al. [5,6], Aurbach and Gofer [7] and Ein-Eli and Aurbach [8] to study lithium surfaces in different liquid electrolytes. Nevertheless, the cells (Li/electrolyte/Li or Ni) had to be dismantled, and the lithium washed and dried (no cooling system was provided) before its introduction into the SEM. Other SEM investigation attempts of various Li-cells [10] did require a washing, and an efficient drying of the samples prior to examination since the authors did not use any special transfer/cooling systems. In both cases, the effect of the extra washing step of the studied surface is always the subject of controversies. Finally, in situ optical microscopy studies of lithium surfaces upon cycling were recently carried out [3,4,9,15], with, however, a lower resolution. The main interest of our semi in situ technique resides in the fact that the battery samples are (1) never exposed to air, and (2) freezed by means of a Peltier-element, thereby preventing the removal of the electrolyte from the battery during the operations under vacuum. However it is generally accepted until now that an air exposure during a few seconds might not change the morphology of the sample. For instance, recent TEM results [14] have shown that a fresh dendrite exposed to air for a few seconds totally loses its crystallinity while globally maintaining its shape.

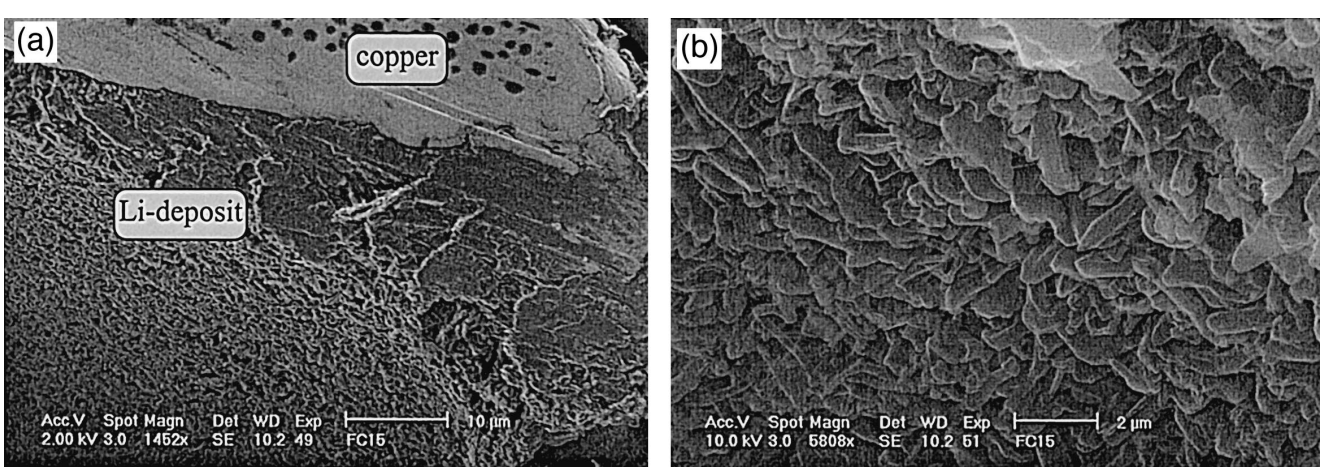

Fig. 12. Cu-surface of a copper cell after one charge at $C/1.7$ (2.6 mA/cm^2), general view (a) and detailed view (b).

Table 1
Li-deposit morphologies after the first charge for different cells and cycling rates

Cell kind	Cycling rate	Current density	Anode/electrolyte interface
lithium battery	$C/5$	0.45 mA/cm^2	moss
	C	2.2 mA/cm^2	dendrites
copper cell	$C/10$	0.45 mA/cm^2	moss
	$C/1.7$	2.6 mA/cm^2	dendritic moss
lithium ion battery	$2C$, C, $C/5$	< 0.1 mA/cm^2	roughness

In short, our transfer method guarantees reliable results, as well as for the profile than for the structure and the chemical nature of the samples.

In spite of the different experimental set-ups between these studies and ours, they all indicated, when looking at the Li-deposition morphology upon cycling, the same lithium morphologic change from moss → bulge → dendrite with increasing charge current density. Thus, our SEM study of lithium cells confirms previous findings while providing more details/features on the interface morphology from the obtaining of sharp SEM micrographs. To our knowledge, the shape of three-dimensional dendrites was never reported with such a fine resolution and sharpness.

Within coin or Swagelok™ cells, the interface contacts are ensured by means of a physical pressure that could modify the Li dendrite growth, and favor homogeneous lithium-deposition. To circumvent this issue, we have implemented the plastic technology approach to the fabrication of a Li-metal battery. Despite the encountered difficulties, such a cell configuration is very convenient to study the formation of dendrites at an interface free of external pressure. Indeed, the Li/(polymer electrolyte) contact was only ensured by the NMP, and the help of the external separator, which did not lead to a strong physical pressure at the Li/separator interface. In addition, because of the special laminated configuration, it was not necessary to dismantle the cell to observe the dendrites, contrary to most of the reported SEM studies [3,5–8,10].

This study has revealed a rapid decrease in the capacity upon cycling. The deterioration of the lithium–polymer interface upon cycling was confirmed by AC-impedance measurements that showed an increase in the interface resistance with increasing cycle numbers (Fig. 14). These Nyquist plots represent the impedances of a complete lithium battery cycled at $C/5$ and stopped after a determined cycle number at the charged state. At the beginning of the cycling two semicircles are obtained: the first one, at low frequencies, probably corresponds to a charge transfer process, while the second one, at high frequencies, is likely due to the ionic conductivity of passivating layers. The straight line at very low frequencies is characteristic of the diffusion, essentially through the cathode. By considering the series of the spectra, it is clear that the total resistance of the cell drastically increases when the capacity rapidly

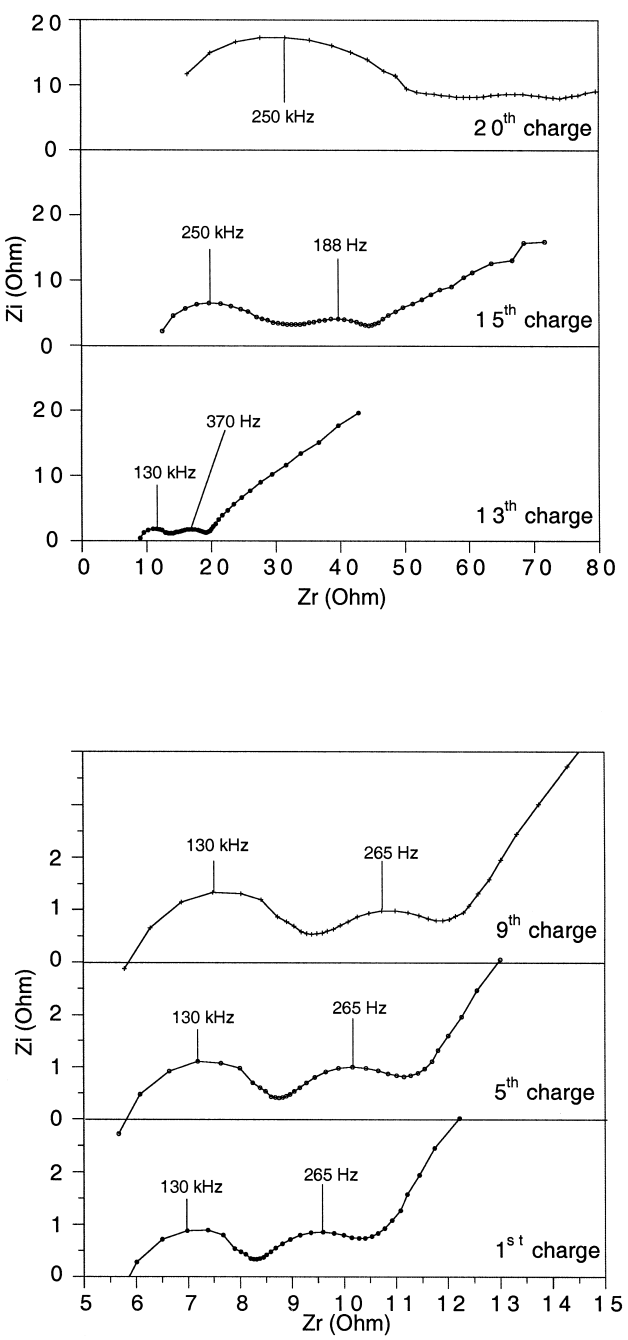

Fig. 14. Nyquist plots of lithium battery cycled at $C/5$ frequency range: 50 mHz–1 MHz.

decreases. The most important contribution of the spectra changes is due to the Li/separator interface, since the other parts, common to the well-known lithium ion battery, do not drastically evolve after 20 cycles. The loss of Li/separator contact is then represented by the irreversible increase in impedance values plotted Fig. 14. This interface deterioration is inherent to the cell configuration reported here that was purposely designed to favor dendrite growth rather than obtain a long-life battery. Indeed, rechargeable Li–polymer batteries with better cycling efficiencies (200 cycles) can be obtained by improving the Li–polymer interfaces using sophisticated technologies, such as in situ or plasma polymerization [16,14], electron beam deposition [17], or rf magnetron sputtering followed by Li thermal evaporation [18]. Rechargeable dry-polymer Li batteries based on PEO were reported to even exceed 1000 cycles at 80°C [19]. These latter configurations are still far from the Li/PVdF–EC–DMC–$LiPF_6$ system which was the topic of our study.

6. Conclusion

The present study performed on both lithium batteries and copper cells has shown a direct correlation between current density and dendrite formation with the largest amount of dendritic deposits formed at high currents. The formation of the mossy or dendritic interface was evidenced to be at the origin of the rapid deterioration of the Li/electrolyte interface, and thereby of the rapid capacity decrease observed. Further investigations are in progress to accurately correlate the SEM micrographs to impedance measurements as well as to determine a solution to suppress the dendrites upon further storage or cycling of the cells.

References

[1] S. Tobishima, Y. Sakurai, J. Yamaki, J. Power Sources 68 (1997) 455.
[2] M.B. Armand, J.M. Chabagno, M.J. Duclot, Second International Conference on Solid Electrolyte, St. Andrews, paper 6.5, 1978.
[3] M. Arakawa, S. Tobishima, Y. Nemoto, M. Ichimura, J. Yamaki, J. Power Sources 43–44 (1993) 27.
[4] Z. Takehara, Z. Ogumi, Y. Uchimoto, K. Yasuda, H. Yoshida, J. Power Sources 43–44 (1993) 377.
[5] D. Aurbach, Y. Gofer, M. Ben-Zion, P. Aped, J. Electroanal. Chem. 339 (1992) 451.
[6] D. Aurbach, Y. Gofer, J. Langzam, J. Electrochem. Soc. 136 (1989) 3198.
[7] D. Aurbach, Y. Gofer, J. Electrochem. Soc. 138 (1991) 3529.
[8] Y. Ein-Eli, D. Aurbach, J. Power Sources 54 (1995) 281.
[9] C. Brissot, M. Rosso, J.N. Chazalviel, P. Baudry, S. Lascaud, Joint International Meeting, Paris, 1997.
[10] T. Osaka, T. Momma, Y. Matsumoto, Y. Uchida, J. Electrochem. Soc. 144 (1997) 1709.
[11] D. Aurbach, Y. Cohen, J. Electrochem. Soc. 144 (1997) 3355.
[12] A.S. Gozdz, J.-M. Tarascon, C.N. Schmutz, U.S. Patent 5,296,318.
[13] A. Blyr, C. Sigala, G. Amatucci, D. Guyomard, Y. Chabre, J.-M. Tarascon, J. Electrochem. Soc. 145 (1998) 194.
[14] N. Langenhuizen et al., J. Electrochem. Soc. (to be published).
[15] T. Osaka, T. Homma, T. Momma, H. Yarimizu, J. Electroanal. Chem. 421 (1997) 153.
[16] T. Matsui, K. Tekeyama, Electrochimica Acta 40 (1995) 2165.
[17] S.D. Jones, J.R. Akridge, F.K. Shokoohi, Solid State Ionics 69 (1994) 357.
[18] J.B. Bates, N.J. Dudney, G.R. Gruzalski, R.A. Zuhr, A. Choudhury, C.F. Luck, J. Power Sources 43–44 (1993) 103.
[19] M. Gauthier, D. Fauteux, G. Vassort, A. Bélanger, M. Duval, P. Ricoux, J.-M. Chabagno, D. Muller, P. Rigaud, M. Armand, D. Deroo, J. Electrochem. Soc. 132 (1985) 1333.